



Champneys, AR., Kuznetsov, YA., & Sandstede, B. (1995). *A numerical toolbox for homoclinic bifurcation analysis*.
<https://doi.org/10.1142/S0218127496000485>

Early version, also known as pre-print

Link to published version (if available):
[10.1142/S0218127496000485](https://doi.org/10.1142/S0218127496000485)

[Link to publication record on the Bristol Research Portal](#)
PDF-document

University of Bristol – Bristol Research Portal

General rights

This document is made available in accordance with publisher policies. Please cite only the published version using the reference above. Full terms of use are available:
<http://www.bristol.ac.uk/red/research-policy/pure/user-guides/brp-terms/>

A Numerical Toolbox for Homoclinic Bifurcation Analysis

A.R. Champneys*, Yu.A. Kuznetsov[†] and B. Sandstede[‡]

Abstract

This paper presents extensions and improvements of recently developed algorithms for the numerical analysis of orbits homoclinic to equilibria in ODEs and describes the implementation of these algorithms within the standard continuation package AUTO86. This leads to a kind of toolbox, called HOMCONT, for analysing homoclinic bifurcations either as an aid to producing new theoretical results, or to understand dynamics arising from applications. This toolbox allows the continuation of codimension-one homoclinic orbits to hyperbolic or non-hyperbolic equilibria as well as detection and continuation of higher-order homoclinic singularities in more parameters. All known codim 2 cases that involve a unique homoclinic orbit are supported. Two specific example systems from ecology and chemical kinetics are analysed in some detail, allowing the reader to understand how to use the toolbox for themselves. In the process, new results are also derived on these two particular models.

1 Introduction

Since the pioneering works of L.P. Shil'nikov in the 1960's, much is now understood about codimension-one bifurcations caused by the existence of an orbit homoclinic to an equilibrium in ODEs. However, in the course of application of these results to specific systems, one generally would like to continue loci of such homoclinic orbits in two or more parameters, thus encountering various codimension-two degeneracies. These codimension-two bifurcations have received a lot attention recently both theoretically (e.g. Lukyanov (1982), Nozdrachova (1982),

*Department of Engineering Mathematics, University of Bristol, Bristol, BS8 1TR, UK

[†]Dynamical Systems Laboratory, Centrum voor Wiskunde en Informatica, P.O.Box 94079, 1090 GB Amsterdam, The Netherlands & Institute of Mathematical Problems of Biology, Russian Academy of Sciences, Pushchino, Moscow Region, 142292 Russia

[‡]Weierstraß-Institut für Angewandte Analysis und Stochastik, Mohrenstraße 39, 10117 Berlin, Germany

Turaev (1988), Belyakov & Shil'nikov (1990), Chow, Deng & Fiedler (1990), Kisaka, Kokubu & Oka (1993), Deng (1993), Homburg, Kokubu & Krupa (1994), Sandstede (1993)) and in applications (see, for example, the recent proceedings Gaspard, Arnéodo, Kapral & Sparrow (1993)). More complete reviews can be found in Fiedler (1992) and Champneys & Kuznetsov (1994), to which we also direct the reader for two-parameter bifurcation diagrams respective to these codim 2 points.

Application of these theoretical results to example systems has always been difficult, typically involving a large amount of numerical computation using *ad hoc* methods. The early numerical methods for locating homoclinic orbits relied on either continuation of a limit cycle to large period as it approaches a homoclinic orbit (Doedel & Kernévez (1986)), or the use of *shooting*, that is, the numerical integration of orbits in the stable and unstable manifolds of the equilibrium and the computation of a distance between them (see, for example, Kuznetsov (1983, 1990), Rodríguez-Luis, Freire & Ponce (1990)). Both of these techniques can be extended to continue homoclinic loci in two parameters.

Boundary-value methods, which are free from instabilities of the mentioned methods due to the strong divergence of trajectories near saddle-type equilibria, date back to Hassard (1980) and Miura (1982), and have been recently analysed and improved by Beyn (1990*b*, 1990*a*), Doedel & Friedman (1989), Friedman (1993), Friedman & Doedel (1991, 1993), Doedel, Friedman & Monteiro (1993), Canale (1994), Schechter (1993, 1994) and Sandstede (1995*b*, 1995*c*) among others. Such methods truncate the homoclinic problem to a finite time interval and impose certain boundary conditions at the end points of that interval. These methods, which have been derived in the more general context of heteroclinic orbits, have been successfully applied to the continuation in two parameters of homoclinic orbits satisfying certain non-degeneracy conditions, i.e. orbits of *codimension one*.

In Champneys & Kuznetsov (1994) an implementation in AUTO86 (Doedel & Kernévez 1986) was described of a version of Beyn's continuation algorithm based on *projection boundary conditions*. The main emphasis of that paper was the automatic accurate location of certain *codimension-two* homoclinic singularities and their continuation in three or more parameters. This was achieved by constructing test functions which are monitored along codim 1 homoclinic curves, the zeroes of which define the relevant codim 2 points. Continuation in three parameters is performed by appending one of these test functions to the continuation problem. The codimension-two singularities treated include all known cases where there is a unique homoclinic orbit to a hyperbolic equilibrium. Test functions for certain global degeneracies, the so-called *orbit-* and *inclination-flip* bifurcations, were derived for the first time for general

n -dimensional systems. The latter of these involves the simultaneous solution of a nonlinear normalised adjoint variational equation around the homoclinic orbit, in order to compute the *orientation* or *twistedness* of the homoclinic loop.

Since then a number of improvements and extensions of the algorithms have been developed. A generalisation to treat codim 1 saddle-node homoclinic orbits was given in Bai & Champneys (1994). In Champneys, Härterich & Sandstede (1995) this method was applied to the computation of a new codim 2 homoclinic bifurcation which leads to the genesis of the less famous, but equally important, codim 1 “Shil’nikov phenomenon” where two homoclinic orbits exist to the same non-hyperbolic equilibrium (Shil’nikov 1969). In the mean while, new improved test functions for inclination and orbit flips have been derived by Sandstede (1995*c*), which for the inclination flip involve solving a modified linear adjoint variational equation, and for which non-degeneracy and convergence were proved. In Sandstede (1995*a*), a method was presented for constructing systems exhibiting certain codim 2 homoclinic singularities, including the first example we are aware of to be proved to exhibit an orbit flip bifurcation.

The present paper collates these recent developments and describes their implementation into HOMCONT¹, a new unified toolbox for numerical homoclinic bifurcation analysis as a supplement to the boundary-value continuation software AUTO86 (Doedel & Kernévez 1986). Specifically, we describe an implementation of the projection boundary condition method applicable to both hyperbolic and saddle node homoclinic orbits, combining the algorithm described in Champneys & Kuznetsov (1994) to an improved version of the algorithm in Bai & Champneys (1994). A more robust method is used for the computation of projection boundary conditions, based on Schur decomposition, that avoids the complications caused by multiple eigenvalues of the Jacobian matrix. The methods from (Sandstede 1995*c*) for computing orbit and inclination flips are also described and implemented. In particular, this leads to a greatly simplified procedure, compared with that in Champneys & Kuznetsov (1994), for generating initial data for the continuation of solutions necessary for computing orientation. We also discuss some new insights into the continuation through saddle-node degeneracies, showing that accurate location and switching between saddle and saddle-node homoclinic continuation is possible. More details on how to run HOMCONT can be found in the accompanying manual Champneys, Kuznetsov & Sandstede (1995).

The outline of the rest of the paper is as follows. In section 2 we describe a unified algorithm for continuation of hyperbolic and non-hyperbolic homoclinic orbits, including computation of

¹available from the authors on request.

orientation where necessary. In particular, we list the test functions used for detection and continuation of all supported codim 2 points. For each test function we discuss its regularity as the truncation time interval $T \rightarrow \infty$. Specific improvements on previous algorithms are highlighted. Section 3 describes the implementation of these methods in HOMCONT as well as the general strategy used for running the driver. Section 4 contains numerical results on two example systems: a planar system arising from ecological modelling and a three-variable system proposed as a phenomenological model of chemical kinetics. In each case we present a detailed step-by-step analysis of homoclinic bifurcations for the purpose of illustrating the use of the driver. Nonetheless the results presented are largely new including two unanalysed codim 3 situations, namely a non-transverse and a critically twisted non-central saddle-node homoclinic orbit. Finally, in Section 5 we draw conclusions and indicate the directions of future work.

2 Algorithm

In this section we briefly summarize algorithms to continue codim 1 homoclinic orbits and to detect codim 2 singularities along their loci.

2.1 Continuation of Codimension-One Homoclinic Orbits

Consider the following boundary-value problem on an infinite interval

$$f(x^*, \alpha) = 0, \tag{2.1}$$

$$\dot{x}(t) = f(x(t), \alpha), \tag{2.2}$$

$$x(t) \rightarrow x^* \text{ as } t \rightarrow \pm\infty. \tag{2.3}$$

Here $f : \mathbb{R}^n \times \mathbb{R}^p \rightarrow \mathbb{R}^n$ is sufficiently smooth. If a pair $\{x^*, x(\cdot)\}$ satisfies the problem (2.1) – (2.3) at some parameter value α , then x^* is an equilibrium of (2.2) and $x(t)$ is a homoclinic solution to this equilibrium. Since any time shift of the solution $x(t)$ is still a solution, a condition is required to fix the phase. Suppose that some initial guess $\tilde{x}(t)$ for the solution is known, then the following integral phase condition

$$\int_{-\infty}^{\infty} \dot{x}^T(t)[x(t) - \tilde{x}(t)]dt = 0 \tag{2.4}$$

is a necessary condition for a minimum of the L_2 -distance between x and \tilde{x} over time shifts (Doedel 1981). Depending on the equilibrium type, one may have to add extra conditions

to (2.1)–(2.4), to obtain a well-posed codim 1 problem, specifying, for example, a curve on a two-parameter plane.

The boundary-value problem (2.1)–(2.4) defined on an infinite time-interval can be approximated by truncation to a finite interval $[-T, +T]$, with suitable boundary conditions as follows (see Beyn (1990*b*, 1990*a*)). Suppose that $A(x^*, \alpha) = (D_x f)(x^*, \alpha)$ has n_s eigenvalues (counting multiplicities) with negative real part, n_0 eigenvalues with zero real part, and n_u eigenvalues with positive real part, so that

$$n_s + n_0 + n_u = n.$$

In the hyperbolic case, $n_0 = 0$, while if the equilibrium x^* is a saddle-node, one has $n_0 = 1$.

Replace (2.3) by the *projection boundary conditions*:

$$L_s(x^*, \alpha)(x(-T) - x^*) = 0, \quad (2.5)$$

$$L_u(x^*, \alpha)(x(+T) - x^*) = 0. \quad (2.6)$$

Here $L_s(x^*, \alpha)$ is a $(n_s \times n)$ matrix whose rows form a basis for the stable eigenspace of $A^T(x^*, \alpha)$. Accordingly, $L_u(x^*, \alpha)$ is a $(n_u \times n)$ matrix, such that its rows form a basis for the unstable eigenspace of $A^T(x^*, \alpha)$. The boundary conditions (2.5) and (2.6) place the solution at the two end points in the center-unstable and center-stable eigenspaces of $A(x^*, \alpha)$, respectively. Notice that a homoclinic solution belongs asymptotically to these eigenspaces as $t \rightarrow \pm\infty$. Finally, take the phase condition of the truncated problem to be

$$\int_{-T}^T \dot{\tilde{x}}^T(t)[x(t) - \tilde{x}(t)]dt = 0. \quad (2.7)$$

It is not difficult to see that the truncated problem (2.1), (2.2), (2.6), and (2.7) is a formally well-posed codim 1 problem, when x^* is *hyperbolic*, since one has n boundary conditions (2.5) and (2.6) plus one integral constraint (2.7). Moreover, under certain regularity conditions (see Beyn (1990*b*, 1990*a*)), the existence of a homoclinic solution to the original problem on the infinite interval implies the existence of a solution to the truncated problem. Furthermore, as $T \rightarrow \infty$, the solution to the truncated problem converges to that of the original one restricted to an appropriate finite interval. The rate of convergence is proved to be exponential for both parameter values and solutions (Beyn 1990*b*, Schechter 1994, Sandstede 1995*b*).

If x^* is a *saddle-node*, (2.5) and (2.6) give only $(n - 1)$ boundary conditions. Thus, an extra equation is required, namely the one defining the saddle-node bifurcation, e.g.

$$\det A(x^*, \alpha) = 0. \quad (2.8)$$

Existence and convergence results are incomplete in this case. However, some theoretical arguments and numerical experiments (see Friedman (1993), Schechter(1993, 1994), Bai & Champneys (1994), Canale (1994), Sandstede (1995b)) suggest that the convergence is exponential in parameters, but that the error for the solutions behaves as $1/T^2$, as $T \rightarrow \infty$.

Solutions to the resulting boundary-value problems can be continued using existing standard software (see Section 3). In the continuation setting, the reference solution $\tilde{x}(t)$ is merely the homoclinic solution obtained at the previously found point on the curve.

2.2 Test Functions for Codimension-Two Bifurcations

Codimension-two homoclinic orbits are detected along branches of codim 1 homoclinics by locating zeroes of certain test functions ψ_i defined in general for an appropriate truncated problem. In the simplest cases, test functions are computable via eigenvalues of the equilibrium or their eigenvectors and from the homoclinic solution at the endpoints. In other cases one has to enlarge the boundary-value problem and simultaneously solve variational equations with relevant boundary conditions. Codim 2 singularities can then be continued by appending the test function to the problem and activating one more parameter.

A test function is said to be *well-defined* if, for all sufficiently large $T > 0$, it is a smooth function along the solution curve of the truncated problem and has a regular zero approaching the critical parameter value as $T \rightarrow \infty$. In fact, in all cases presented below, we have the stronger property that the limit of the test function exists and gives a regular test function for the original problem on the infinite interval also.

To start with we denote the eigenvalues of $A(x^*, \alpha) = D_x f(x^*, \alpha)$ with negative real part as

$$\mu_i, \quad i = 1, 2, \dots, n_s,$$

the eigenvalues with zero real part as

$$\gamma_j, \quad j = 1, 2, \dots, n_0,$$

and the eigenvalues with positive real part as

$$\lambda_k, \quad k = 1, 2, \dots, n_u.$$

We assume that the non-critical eigenvalues are ordered according to

$$\operatorname{Re} \mu_{n_s} \leq \dots \leq \operatorname{Re} \mu_1 < 0 < \operatorname{Re} \lambda_1 \leq \dots \leq \operatorname{Re} \lambda_{n_u}. \quad (2.9)$$

The eigenvalues with zero real part are called *central*, while the stable (unstable) eigenvalues with real part closest to zero are termed the *leading* stable (unstable) eigenvalues.

2.2.1 Singularities detectable via eigenvalues

The following test functions can be monitored along a homoclinic curve corresponding to a hyperbolic equilibrium to detect codim 2 singularities which were shown in Champneys & Kuznetsov (1994) to be well-defined for both the original and truncated problems.

Resonant saddle:

$$\psi_1 = \mu_1 + \lambda_1. \quad (2.10)$$

Double real stable leading eigenvalue:

$$\psi_2 = \begin{cases} (\operatorname{Re}\{\mu_1\} - \operatorname{Re}\{\mu_2\})^2, & \operatorname{Im}\{\mu_1\} = 0, \\ -(\operatorname{Im}\{\mu_1\} - \operatorname{Im}\{\mu_2\})^2, & \operatorname{Im}\{\mu_1\} \neq 0. \end{cases} \quad (2.11)$$

Double real unstable leading eigenvalue:

$$\psi_3 = \begin{cases} (\operatorname{Re}\{\lambda_1\} - \operatorname{Re}\{\lambda_2\})^2, & \operatorname{Im}\{\lambda_1\} = 0, \\ -(\operatorname{Im}\{\lambda_1\} - \operatorname{Im}\{\lambda_2\})^2, & \operatorname{Im}\{\lambda_1\} \neq 0. \end{cases} \quad (2.12)$$

Notice that the regularity of (2.11) and (2.12) follows from the fact that these expressions represent the discriminant of the quadratic factor of the characteristic polynomial corresponding to this pair of eigenvalues.

Neutral saddle, saddle-focus or bi-focus:

$$\psi_4 = \operatorname{Re}\{\mu_1\} + \operatorname{Re}\{\lambda_1\}. \quad (2.13)$$

Neutrally-divergent saddle-focus

$$\psi_5 = \operatorname{Re}\{\mu_1\} + \operatorname{Re}\{\mu_2\} + \operatorname{Re}\{\lambda_1\}, \quad (2.14)$$

$$\psi_6 = \operatorname{Re}\{\lambda_1\} + \operatorname{Re}\{\lambda_2\} + \operatorname{Re}\{\mu_1\}. \quad (2.15)$$

Three leading eigenvalues

$$\psi_7 = \operatorname{Re}\{\mu_1\} - \operatorname{Re}\{\mu_3\}, \quad (2.16)$$

$$\psi_8 = \operatorname{Re}\{\lambda_1\} - \operatorname{Re}\{\lambda_3\}. \quad (2.17)$$

In order to detect homoclinic orbits to non-hyperbolic equilibria while continuing a locus of hyperbolic homoclinics, the truncated problem should be formulated in such a way that it can be continued *through* the degenerate point. To this end it is necessary to modify the labelling (2.9) to label as μ_i the n_s leftmost eigenvalues and as λ_i the n_u rightmost eigenvalues irrespective of their location with respect to the imaginary axis. This accordingly modifies the

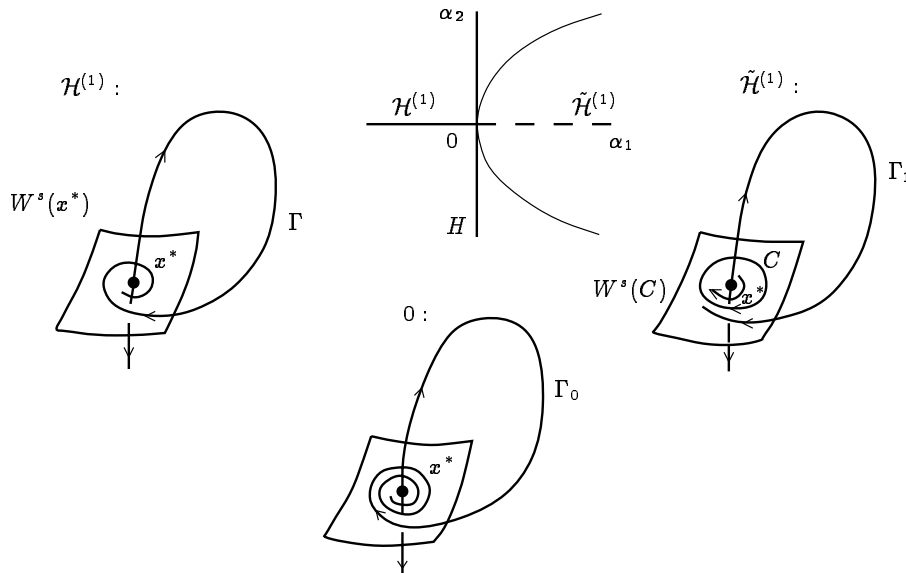


Figure 1: Continuation through a Shil'nikov-Hopf with $n = 3$. The homoclinic locus is denoted by $\mathcal{H}^{(1)}$ and the point-to-periodic heteroclinic curve by $\tilde{\mathcal{H}}^{(1)}$.

meaning of the terms “stable” and “unstable” in the definition² of the projection matrices $L_{u,s}$. With this modification, we can simply define the following test functions.

Non-hyperbolic equilibria:

$$\psi_9 = \operatorname{Re}\{\mu_1\}, \quad (2.18)$$

$$\psi_{10} = \operatorname{Re}\{\lambda_1\}. \quad (2.19)$$

A zero of $\psi_{9,10}$ corresponds to either a fold or Hopf bifurcation³ of the continued equilibrium x^* . In the first case the bifurcation is called a *non-central saddle-node homoclinic* bifurcation (see below), while the second one is usually referred to as a *Shil'nikov-Hopf* bifurcation. Generically these singularities are end points of a locus of homoclinic orbits to hyperbolic equilibria. However, there exist continuous extensions of the solution curves of the truncated boundary-value problem (2.1), (2.2), (2.5)–(2.7) through both singularities. This fact was pointed out for the Shil'nikov-Hopf case in Champneys & Kuznetsov (1994), where it was noted that beyond the codim 2 point, there exists a solution curve $\tilde{\mathcal{H}}^{(1)}$ approximating a *heteroclinic connection* Γ_1 between x^* and the limit cycle C appearing via the Hopf bifurcation. See Figure 1 for an illustration in three dimensions.

²In HOMCONT the user specifies in advance the numbers n_u and n_s to be used throughout a particular continuation.

³We do not consider pitchfork or transcritical bifurcations here, as these are of a higher codimension for generic dynamical systems.

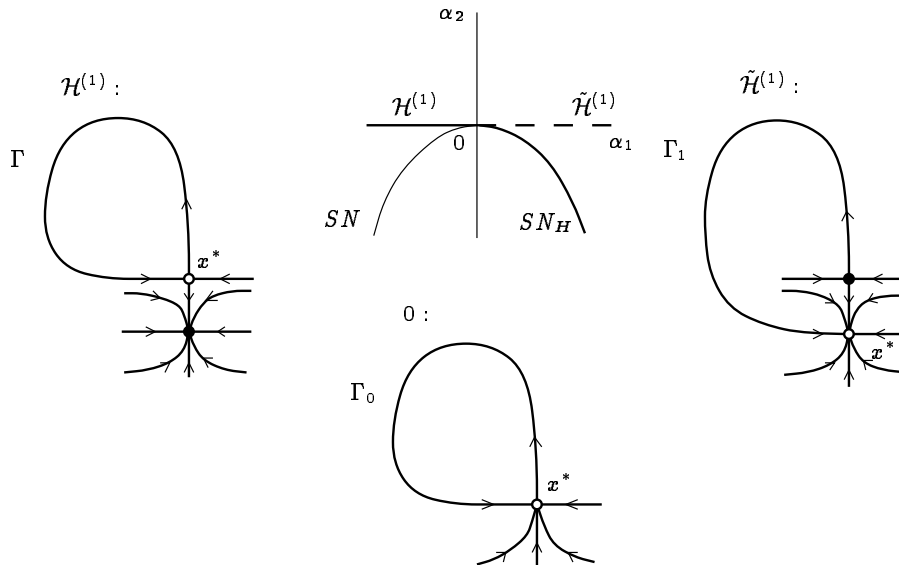


Figure 2: Continuation through a non-central saddle-node homoclinic bifurcation. The hyperbolic homoclinic curve is denoted by $\mathcal{H}^{(1)}$, the non-central heteroclinic curve by $\tilde{\mathcal{H}}^{(1)}$ and the curve of folds by SN . Along the right-hand branch SN_H of the fold curve there also exists a central saddle-node homoclinic.

It turns out that a similar property holds for the saddle-node bifurcation, contrary to a statement in Champneys & Kuznetsov (1994), provided an appropriate truncated problem is used for continuation. Suppose we continue a saddle homoclinic locus $\mathcal{H}^{(1)}$ towards a fold bifurcation of x^* , which means that an extra equilibrium approaches x^* . For simplicity we assume that at the saddle-node point an unstable eigenvalue approaches zero, see Figure 2 for a planar illustration. Beyond the codim 2 point, the truncated boundary-value problem has a solution approximating a heteroclinic orbit connecting the two equilibria along the non-leading stable manifold and existing along $\tilde{\mathcal{H}}^{(1)}$. More precisely, the continuation algorithm switches from the original equilibrium to the approaching one⁴, while the projection boundary conditions place the end points of the solution in the “stable” and “unstable” eigenspaces of the new x^* . Close to the codim 2 point, the latter gives a good approximation to the unstable eigenspace of the original equilibrium.

2.2.2 Orbit and inclination flips

We now consider test functions for two forms of *global* degeneracy along a curve of homoclinic orbits to a saddle, namely *orbit-* and *inclination-flip* bifurcations. Therefore we additionally

⁴Beyond the critical point it is the approaching equilibrium that is labelled x^* .

assume that there are no center eigenvalues of $A(x^*, \alpha)$, while the leading eigenvalues are real and unique, that is

$$\operatorname{Re} \mu_{n_s} \leq \cdots \leq \operatorname{Re} \mu_2 < \mu_1 < 0 < \lambda_1 < \operatorname{Re} \lambda_2 \leq \cdots \leq \operatorname{Re} \lambda_{n_u}.$$

Then, it is possible to choose normalised eigenvectors w_1^s and w_1^u of $A^T(x^*, \alpha)$ depending smoothly on (x^*, α) and satisfying

$$A^T(x^*, \alpha) w_1^s = \mu_1 w_1^s \quad A^T(x^*, \alpha) w_1^u = \lambda_1 w_1^u.$$

Here and in what follows the dependence on x^* and α of eigenvalues and eigenvectors is not indicated, for simplicity. Accordingly, normalised eigenvectors v_1^s and v_1^u of $A(x^*, \alpha)$ are chosen depending smoothly on (x^*, α) and satisfying

$$A(x^*, \alpha) v_1^s = \mu_1 v_1^s \quad A(x^*, \alpha) v_1^u = \lambda_1 v_1^u.$$

An orbit flip bifurcation occurs when the homoclinic orbit changes its direction of approach to the saddle between the two components of a leading eigenvector. The defining equation for the orbit-flip bifurcation (with respect to the stable manifold) can be written as

$$\lim_{t \rightarrow \infty} e^{-\mu_1 t} \langle w_1^s, x(t) - x^* \rangle = 0, \quad (2.20)$$

where $\langle a, b \rangle = a^T b$ is the standard scalar product of $a, b \in \mathbb{R}^n$. Similarly, the equation for the orbit-flip with respect to the unstable manifold is given by

$$\lim_{t \rightarrow -\infty} e^{-\lambda_1 t} \langle w_1^u, x(t) - x^* \rangle = 0. \quad (2.21)$$

At a point where either condition (2.20) or (2.21) is fulfilled, the homoclinic orbit tends to the saddle (in one time direction) along its nonleading eigenspace (see Sandstede (1995c) for the details).

The truncated test functions are therefore given by

Orbit-flip (with respect to the stable manifold):

$$\psi_{11} = e^{-\mu_1 T} \langle w_1^s, x(+T) - x^* \rangle = 0. \quad (2.22)$$

Orbit-flip (with respect to the unstable manifold):

$$\psi_{12} = e^{\lambda_1 T} \langle w_1^u, x(-T) - x^* \rangle = 0. \quad (2.23)$$

Note that the projections and the scaling appearing in (2.22) and (2.23) are different from those used in Champneys & Kuznetsov (1994).

The inclination-flip bifurcation is related to global twistedness of the stable and unstable manifolds $W^{s,u}(x^*)$ of the saddle x^* around its homoclinic orbit. At each point $x(t)$ of the homoclinic orbit the sum of tangent spaces

$$Z(t) = X(t) + Y(t)$$

is defined, where

$$X(t) = T_{x(t)}W^s(x^*), \quad Y(t) = T_{x(t)}W^u(x^*).$$

Generically, $\text{codim } Z(t) = 1$, that is $X(t) \cap Y(t) = \text{span}\{\dot{x}(t)\}$.

In order to describe the defining equations for the inclination-flip bifurcation we have to introduce the adjoint variational problem

$$\dot{\varphi} = -(D_x f)^T(x(t), \alpha) \varphi, \quad (2.24)$$

$$\varphi(t) \rightarrow 0 \text{ as } t \rightarrow \pm\infty, \quad (2.25)$$

$$\int_{-\infty}^{\infty} \tilde{\varphi}^T(t) [\varphi(t) - \tilde{\varphi}(t)] dt = 0. \quad (2.26)$$

The “phase condition” (2.26) selects one solution out of the family $c\varphi(t)$ for $c \in \mathbb{R}$. The solution $\varphi(t)$ of (2.24)–(2.26) is orthogonal to the above defined subspace $Z(t)$ for each t , thus, its limit behavior as $t \rightarrow \pm\infty$ determines the twistedness of the space $Z(t)$ around the homoclinic orbit. Inclination-flip bifurcations occur at points along a homoclinic curve where this twistedness changes without an orbit flip occurring (see (Sandstede 1995c, Champneys & Kuznetsov 1994) and references therein for a more detailed explanation). The defining equations for the inclination-flip bifurcation with respect to the stable manifold are given by

$$\lim_{t \rightarrow -\infty} e^{\mu_1 t} \langle v_1^s, \varphi(t) \rangle = 0, \quad (2.27)$$

and with respect to the unstable manifold by

$$\lim_{t \rightarrow \infty} e^{\lambda_1 t} \langle v_1^u, \varphi(t) \rangle = 0. \quad (2.28)$$

If either (2.27) or (2.28) holds, the stable (unstable) manifolds of the saddle x^* are neutrally twisted around the homoclinic orbit (Sandstede 1995c).

Next we define $P_s(x^*, \alpha)$ to be the $(n_s \times n)$ matrix whose rows form a basis for the stable eigenspace of $A(x^*, \alpha)$. Similarly, $P_u(x^*, \alpha)$ is a $(n_u \times n)$ matrix, such that its rows form a basis for the unstable eigenspace of $A(x^*, \alpha)$. Consider now replacing (2.24)–(2.26) by the truncated equations

$$\dot{\varphi} = -(D_x f)^T(x(t), \alpha) \varphi + \varepsilon f(x(t), \alpha), \quad (2.29)$$

$$P_s(x^*, \alpha) \varphi(+T) = 0, \quad (2.30)$$

$$P_u(x^*, \alpha) \varphi(-T) = 0, \quad (2.31)$$

$$\int_{-T}^T \tilde{\varphi}^T(t) [\varphi(t) - \tilde{\varphi}(t)] dt = 0 \quad (2.32)$$

Here, $\varepsilon \in \mathbb{R}$ is an artificial free parameter, which turns (2.29) into a well-posed boundary-value problem. This truncated system was introduced and investigated in Sandstede (1995c). Evaluating the limits in (2.27) and (2.28) at $t = \pm T$, yields the following test functions.

Inclination-flip (with respect to the stable manifold):

$$\psi_{13} = e^{-\mu_1 T} \langle v_1^s, \varphi(-T) \rangle = 0. \quad (2.33)$$

Inclination-flip (with respect to the unstable manifold):

$$\psi_{14} = e^{\lambda_1 T} \langle v_1^u, \varphi(+T) \rangle = 0. \quad (2.34)$$

Note again that the projections and the scaling appearing in (2.33) and (2.34) differ from those used in Champneys & Kuznetsov (1994). The test functions $\psi_{11,12,13,14}$ are well defined for both the original and truncated boundary-value problems (Sandstede 1995c).

2.2.3 Singularities along saddle-node homoclinic curves

Suppose that a central saddle-node homoclinic orbit is continued. Let $\gamma_1 = 0$ be the unique central eigenvalue, i.e. $n_0 = 1$. Recall that in this case the truncated boundary-value problem is composed of equations (2.1), (2.2), (2.5)–(2.8). Let v_1 be an eigenvector corresponding to $\gamma_1 = 0$ and normalised according to

$$v_1^T v_1 = 1.$$

Suppose that v_1 is differentiable along the saddle-node bifurcation curve. Then the following test functions, which differ from those proposed in Bai & Champneys (1994) by the additional scaling factor $1/T$, will detect non-central saddle-node homoclinic orbits.

Non-central saddle-node homoclinic orbit:

$$\psi_{15} = \frac{1}{T} (x(+T) - x^*)^T v_1, \quad (2.35)$$

$$\psi_{16} = \frac{1}{T} (x(-T) - x^*)^T v_1. \quad (2.36)$$

These functions measure the component of the one-dimensional center manifold in which the two endpoints of the approximate homoclinic orbit lie, and are well-defined along the saddle-node bifurcation curve (see Figure 3). Owing to Schecter (1993, Lemma 3.1) both ψ_{15} and

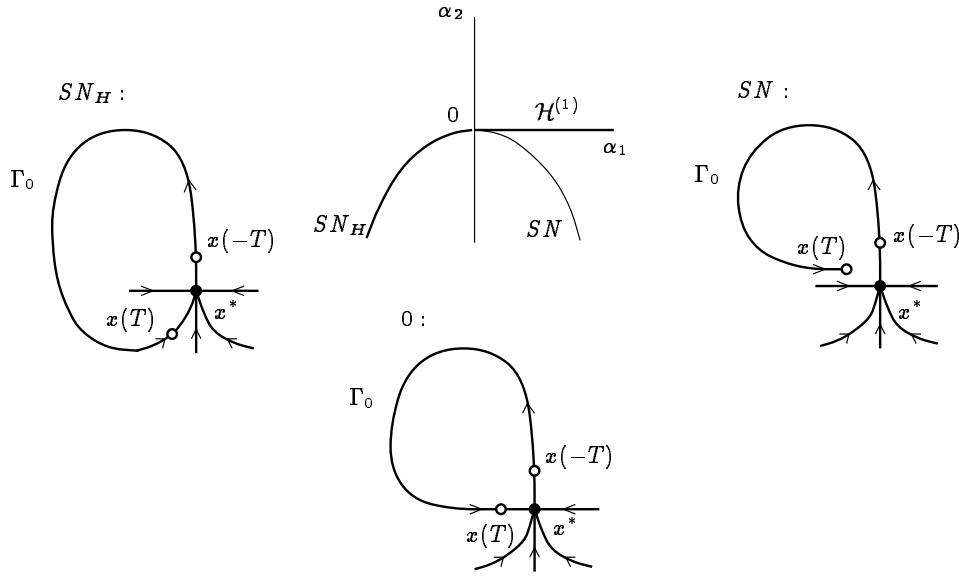


Figure 3: Continuation through a non-central saddle-node homoclinic bifurcation while following a central saddle-node homoclinic curve.

ψ_{16} converge to smooth functions along the curve of central saddle-node homoclinic orbits as $T \rightarrow \infty$. The scaling is similar to the one for the flip bifurcations introduced before. The common feature is to multiply by the correct factor to counteract the asymptotic behavior of the homoclinic solution along the regular branch. This results in smooth defining equations in the limit $T \rightarrow \infty$, see Sandstede (1995c). Which of the test functions (2.35), (2.36) is annihilated is determined by whether the critical homoclinic orbit is a center-to-stable or unstable-to-center connection.

The test-functions $\psi_{9,10}$ and $\psi_{15,16}$ provide us with two different strategies for detecting non-central saddle-node homoclinic orbits. This allows us to switch between the continuation of saddle and central saddle-node homoclinic orbits at such points, as well as giving us two possible methods for continuing such singularities in three parameters.

2.2.4 Other singularities

The test functions listed above do not detect all known codim 2 homoclinic singularities. Clearly, all cases when two homoclinic orbits are present at the critical parameter values are undetectable by monitoring these functions. The same is true for heteroclinic cycles, e.g. when a homoclinic orbit is broken by colliding with an extra equilibrium point. Some more comments are made in the Conclusion. We also do not detect cases when a homoclinic orbit shrinks to an equilibrium at a local codim 2 bifurcation (like at the Bogdanov-Takens singularity). Note,

however, that certain degeneracies which are not formally given a test function may nonetheless be detected and continued using the described algorithm. For example, in Champneys, Härterich & Sandstede (1995) it was shown that a *non-transverse saddle-node homoclinic* bifurcation may be detected as a limit point with respect to the parameter along a curve of central saddle-node homoclinic bifurcations.

3 Implementation

We shall now explain how the algorithms given in the previous section are implemented within the continuation software AUTO86. See (Doedel & Kernévez 1986) and the tutorial papers Doedel, Keller & Kernévez (1991a, 1991b)) for details of the numerical methods used by AUTO86, of the practicalities of using the software and for a list of its capabilities.

3.1 Continuation

Among other things, AUTO can compute paths of solutions to boundary-value problems with integral constraints and non-separated boundary conditions;

$$\dot{U}(\tau) = F(U(\tau), \beta), \quad U(\cdot), F(\cdot, \cdot) \in \mathbb{R}^N, \beta \in \mathbb{R}^{n_{\text{free}}}, \tau \in [0, 1] \quad (3.1)$$

$$b(U(0), U(1), \beta) = 0, \quad b(\cdot, \cdot) \in \mathbb{R}^{n_{\text{bc}}}, \quad (3.2)$$

$$\int_0^1 q(U(\tau), \beta) d\tau = 0, \quad q(\cdot, \cdot) \in \mathbb{R}^{n_{\text{in}}}, \quad (3.3)$$

as n_{free} free parameters β are allowed to vary, where

$$n_{\text{free}} = n_{\text{bc}} + n_{\text{in}} - N + 1. \quad (3.4)$$

The function q is also allowed to depend on F , the derivative of U with respect to pseudo-arclength and on \tilde{U} , the value of U at the previously computed point on the solution branch. Moreover, AUTO86 can accurately locate zeros along the solution branch of functions

$$g_j(U(0), U(1), \beta), \quad j = 1, \dots, n_{\text{uszl}} \quad (3.5)$$

Actually, the user-defined functions in AUTO86 are functions of parameters only (not necessarily just the free parameters). In HOMCONT data is passed between the AUTO86 subroutines USZR and BCND using common blocks, to enable the g_j 's to depend also on the boundary values of U .

To be concrete, suppose we wish to continue solutions to the equations (2.1), (2.2), (2.5)–(2.7) for a homoclinic orbit to a hyperbolic equilibrium together with equations (2.29)–(2.32) for the solution of the modified adjoint variational equation, subject to n_{fix} constraints

$$\psi_i = 0, \quad i = i_{\text{fix}1}, \dots, i_{\text{fix}n_{\text{fix}}},$$

where $i_{\text{fix}j}$ is the label of the j th test function that has been frozen, as $n_{\text{fix}} = n_{\text{free}} + 2$ parameters

$$\alpha_i, \quad i = i_{\text{free}1}, \dots, i_{\text{free}n_{\text{free}}}$$

are allowed to vary. Suppose too that we want to monitor n_{test} test functions

$$\psi_i, \quad i = i_{\text{test}1}, \dots, i_{\text{test}n_{\text{test}}}.$$

Then this problem can be written in the form (3.1)–(3.5) after a suitable time shift and rescaling that identifies $t = -T$ with $\tau = 0$ and $t = T$ with $\tau = 1$. Specifically we have

$$N = 2n, \quad n_{\text{bc}} = 3n + n_{\text{fix}}, \quad n_{\text{in}} = 2, \quad U(\tau) = (x(\tau), \varphi(\tau))^T,$$

$$\beta = (x^*, \varepsilon, \alpha_i, i = i_{\text{free}1}, \dots, i_{\text{free}n_{\text{free}}}),$$

$$F(U, \beta) = \begin{pmatrix} 2T f(x, \alpha) \\ -2T \left([(D_x f)(x, \alpha)]^T \varphi - \varepsilon f(u, \alpha) \right) \end{pmatrix}, \quad (3.6)$$

$$b(U(0), U(1), \beta) = \begin{pmatrix} f(x^*, \alpha) \\ L_s(x^*, \alpha)(x(0) - x^*) \\ L_u(x^*, \alpha)(x(1) - x^*) \\ P_u(x^*, \alpha)\varphi(0) \\ P_s(x^*, \alpha)\varphi(1) \\ \psi_k, k = i_{\text{fix}1}, \dots, i_{\text{fix}n_{\text{fix}}} \end{pmatrix},$$

$$q(U, \beta) = \begin{pmatrix} \dot{x}^T (x - \tilde{x}) \\ \tilde{\varphi}^T (\varphi - \tilde{\varphi}) \end{pmatrix},$$

$$g_i(U(0), U(1), \beta) = \psi_i, \quad i = i_{\text{test}1}, \dots, i_{\text{test}n_{\text{test}}}.$$

Note that the defining equation (2.1) for the equilibrium is treated as a boundary condition. Also, the scaling of time should be taken into account when computing the test functions (2.22), (2.23), (2.33), (2.34).

In the case of saddle-node homoclinics, where one has to solve the problem (2.1), (2.2), (2.5)–(2.8), we do not append the modified variational equation or their boundary and integral conditions and remove the artificial component ε from the parameter β . Instead we keep the same number of free parameters n_{free} and additionally consider one of the boundary conditions to be the defining condition for a saddle-node, which we express as zero of an eigenvalue rather than (2.8).

3.2 Computation of eigenspaces

In order to have a well-posed problem, it is necessary for the boundary conditions to be sufficiently smooth with respect to parameters. Recall that the boundary conditions (2.5), (2.6) and (2.30), (2.31) are defined with respect to bases of the stable or unstable eigenspaces of A or A^T . One approach, adopted in Champneys & Kuznetsov (1994), is to compute the (generalised) eigenvectors in the appropriate eigenspace using a “black box” eigenvalue routine and then to adapt this basis to be smooth with respect to parameters, using a technique due to Beyn (1990*b*, App C.) which amounts to the solution of a linear system of the dimension of the eigenspace in question (see also eqs. (3.8) and (3.9) in Champneys & Kuznetsov (1994)). The drawback of this approach is that we require the black box routine to be intelligent enough to correctly detect multiple eigenvalues and compute generalised eigenvectors there. This poses particular problems when we wish to detect double leading eigenvalue bifurcations (see Section 2.2.1).

The approach used here is instead to extract the necessary basis from the *Schur decomposition* (see, for example (Golub & van Loan 1989)) of the matrix in question, which for definiteness we take to be A . The algorithm, which can be summarised as follows, completely avoids the above complications due to multiple eigenvalues. First, by the use of orthogonal similarity transformations, we reduce A to upper Hessenberg form. This is achieved using the EISPACK routines ORTHES and ORTRAN. Next we use a modified form of the EISPACK routine HQR3, to reduce the upper Hessenberg matrix A to quasi-triangular form by orthogonal similarity transformations. The eigenvalues of A , which are contained in the 1×1 and 2×2 diagonal blocks of the reduced matrix, are ordered in ascending or descending order of their real part along the diagonal according to whether we wish to find a basis for the stable or unstable eigenspace. The superposition of the above transformations are accumulated in a matrix V . The first n_s or n_u columns of V give an orthogonal basis for the stable or unstable eigenspace of A . Unfortunately, this procedure does not guarantee smoothness of the resulting basis with

respect to parameters. Therefore, we employ the above-mentioned Beyn technique for achieving this smoothness.

Note that this Schur-vector technique also works in the saddle-node homoclinic case, because we only ever need the continuity of the stable and unstable eigenspaces of A^T . Thus we never need the null-vector for the boundary conditions. On the contrary we do need the null-vector in order to evaluate the test functions (2.35) and (2.36) for the non-central saddle-node homoclinic bifurcation, and appropriate eigenvectors in order to detect orbit and inclination flips using the test functions (2.22),(2.23), (2.33),(2.34). Moreover, these eigenvectors need also to be continuous along homoclinic loci. This is done by using a standard routine (F02AGF from the NAG library) which computes eigenvectors with unit norm, and then ensuring a positive scalar product with the corresponding eigenvector computed at the previous point. Of course, we also need to compute all the eigenvalues, and to order them with respect to their real parts.

3.3 Starting strategies

We suppose initially that we do not wish to compute the twistedness of the homoclinic loop. Three possible ways of starting the continuation of solutions to (2.1), (2.2), (2.5)–(2.7), are allowed for in HOMCONT. Firstly we suppose that data may be saved from a previous AUTO86 computation of a periodic orbit of large period. In this case, provided the endpoints of the stored data are close to the equilibrium, we simply use the standard restart facility of AUTO86. Secondly, data from a numerical integration of an orbit approximating a homoclinic, obtained for example by a shooting approach (see Kuznetsov (1990)), may be read into AUTO86 in multi-column format. Finally, we allow for use of a *homotopy* approach due to Doedel et al. (1993). This method consists of starting with a small solution in the unstable manifold, performing additional continuation with respect to the truncation interval T , while monitoring the error in the right-hand boundary conditions, and finally performing continuation to make this error zero. These techniques are demonstrated on examples in Section 4 below and in full details in Champneys, Kuznetsov & Sandstede (1995).

In order to compute the twistedness of a homoclinic orbit or inclination-flip bifurcations one needs to solve for the modified adjoint variational equation (2.29), (2.30)–(2.32). Note that this system is affine in φ and that AUTO86 uses Newton's method to solve discretisations of boundary-value problems. Therefore, if the homoclinic solution $x(t)$ were already computed, then Newton's method applied to this affine problem would converge in one step, provided the

initial guess $\tilde{\varphi}$ is chosen such that

$$\int_{-T}^T \tilde{\varphi}^T(t) \varphi(t) dt \neq 0, \quad (3.7)$$

where φ denotes the solution of the original problem (2.24)–(2.26). Note that almost every guess $\tilde{\varphi}$ will satisfy (3.7). In HOMCONT, we provide a facility for appending an initial guess for φ to the data for a homoclinic solution. As such an initial guess we take the constant function

$$\tilde{\varphi}(t) = (0.1, \dots, 0.1)^T.$$

It is easy to modify this subroutine so that the user can incorporate his own initial guess for φ in the same manner. The required single Newton step is made in AUTO86 by performing one step of continuation with respect to a dummy parameter.

Note that it is trivial to start the computation of a saddle homoclinic orbit from a non-central saddle-node bifurcation detected by a zero of (2.18) or (2.19) along a curve of central saddle-node homoclinics, or visa versa, because no extra data is required.

3.4 Running HOMCONT

To run HOMCONT on a new example, the user is only required to specify the right-hand sides of the differential equations, together with their Jacobian derivative, and various constants defining the size of the problem, dimension of stable and unstable manifolds, as well as the kind of computation required including which test functions should be monitored or solved for. All this information is stored in a short FORTRAN programme that is then linked to the HOMCONT library which automatically defines the continuation problem to be solved by AUTO86. Full details, including how to repeat the computations presented below, are presented in Champneys, Kuznetsov & Sandstede (1995).

4 Examples

4.1 Predator-prey model by M. Scheffer

Consider the following system of two equations (Scheffer 1995)

$$\dot{X} = rX \left(1 - \frac{X}{K}\right) - \frac{a_1 XY}{b_1 + X} + d_0 K, \quad (4.1)$$

$$\dot{Y} = e_1 \frac{a_1 XY}{b_1 + X} - d_1 Y - \frac{a_2 Z Y^2}{b_2^2 + Y^2}, \quad (4.2)$$

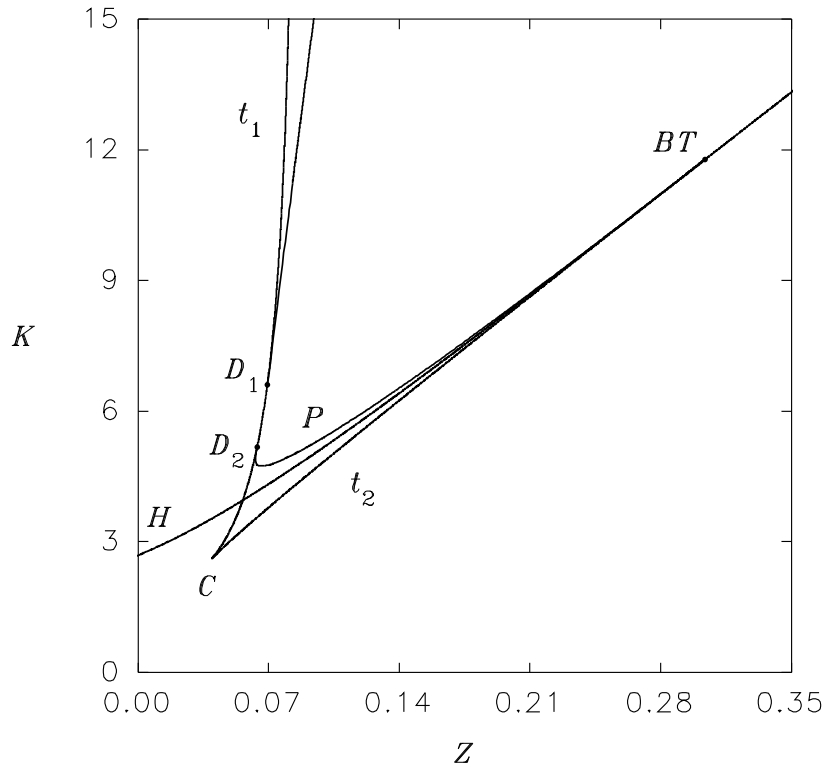


Figure 4: Parametric portrait of the predator-prey system

where X and Y are prey and predator population densities, Z is the density of a super-predator that is kept at a fixed level, while other parameters describe properties of the isolated dynamics of predator and prey and their interaction. The values of all parameters except (K, Z) are set as follows:

$$r = 0.5, \quad a_1 = 0.4, \quad b_1 = 0.6, \quad d_0 = 0.01, \quad e_1 = 0.6, \quad a_2 = 1.0, \quad b_2 = 0.5, \quad d_1 = 0.15.$$

The parametric portrait of the system (4.1), (4.2) on the (Z, K) -plane is presented in Figure 4. It contains fold $(t_{1,2})$ and Hopf (H) bifurcation curves, as well as a homoclinic bifurcation curve P . The fold curves meet at a cusp singular point C , while the Hopf and the homoclinic curves originate at a Bogdanov-Takens point BT . Only the homoclinic curve P will concern us here, the other bifurcation curves were computed using LOCBIF (Khibnik, Kuznetsov, Levitin & Nikolaev 1993) (AUTO86 can be used as well).

4.1.1 Continuation of central saddle-node homoclinics

Local bifurcation analysis shows that at $K = 6.0$, $Z = 0.06729762 \dots$, the system has a saddle-node equilibrium

$$(X^0, Y^0) = (5.738626 \dots, 0.5108401 \dots),$$

with one zero and one negative eigenvalue ($n_s = 1$, $n_u = 0$). Direct simulations reveal a homoclinic orbit to this saddle-node, departing and returning along its central direction (i.e. tangent to the null-vector). For example, a good initial approximation to this orbit can be obtained starting at $(X, Y) = (5.6856, 0.56351)$ and integrating numerically over $T = 1046.178$ units of time.

Starting from this solution, we continue the saddle-node central homoclinic orbit with respect to parameters K and Z , and monitor the test-functions ψ_{15} and ψ_{16} to detect non-central saddle-node homoclinic orbits. The output indicates that a zero of the test function ψ_{15} has been located at

$$D_1 = (K_1, Z_1) = (6.610458 \dots, 0.06932482 \dots),$$

where the homoclinic orbit to the saddle-node becomes *non-central*, namely, it returns to the equilibrium along the stable eigenvector, forming a non-smooth loop. Repeating computations in the opposite direction along the curve, one obtains another non-central saddle-node homoclinic bifurcation at

$$D_2 = (K_2, Z_2) = (5.180308 \dots, 0.06385499 \dots).$$

4.1.2 Switching between saddle-node and saddle homoclinic orbits

Now we can switch to continuation of saddle homoclinic orbits at the located codim 2 points D_1 and D_2 . For this, we fix $n_s = n_u = 1$ and use the standard restart facilities of AUTO86. One can activate the test functions $\psi_{9,10}$ to monitor for nonhyperbolic equilibria along the homoclinic locus. Running HOMCONT from D_1 produces the upper branch of P in Figure 4. Restarting in the opposite direction from the first computed point will detect the same codim 2 point D_1 but now as a zero of the test-function ψ_9 . Actually, the program runs further and eventually computes the point D_2 and the whole lower branch of P emanating from it, however, the solutions between D_1 and D_2 should be considered as spurious. The reliable way to compute the lower branch of P is to restart HOMCONT from the point D_2 in the backward direction. This gives the lower branch of P approaching the Bogdanov-Takens point BT (see Figure 4).

It is worthwhile to compare the homoclinic curves computed above with a curve $T_0 = \text{const}$ along which the system has a limit cycle of constant large period $T_0 = 1046.178$, which can easily be computed using AUTO86 or LOCBIF. Such a curve is plotted in Figure 5. It obviously approximates well the saddle homoclinic loci of P , but demonstrates much bigger deviation from the saddle-node homoclinic segment $D_1 D_2$. This happens, because the period of the limit cycle grows to infinity while approaching both types of homoclinic orbit, but with *different*

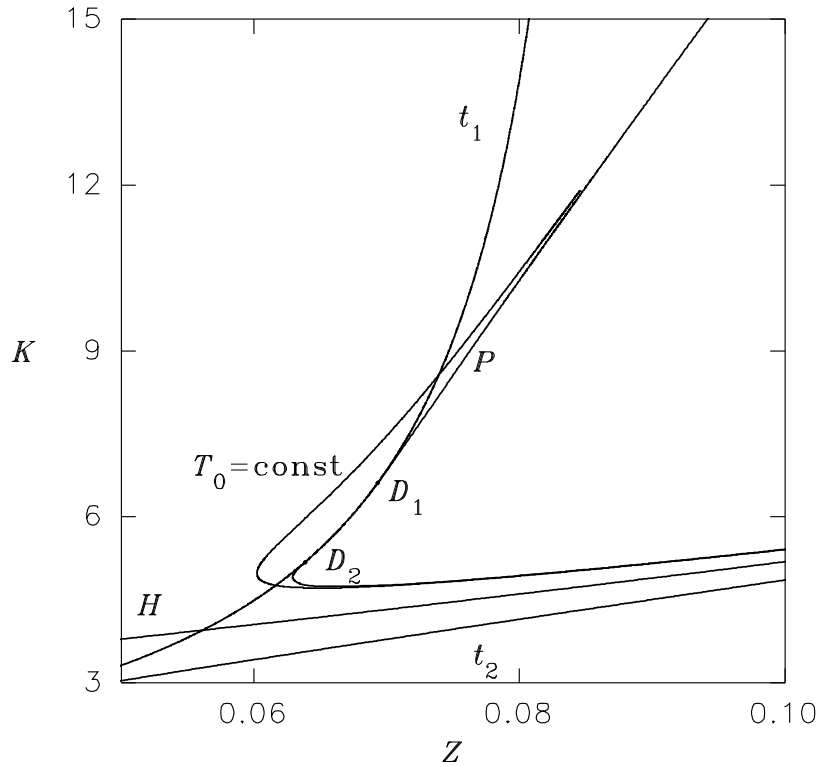


Figure 5: Approximation by a large-period cycle

asymptotics: as $\|\alpha - \alpha^*\|^\gamma$, where $\gamma = \mu_1/\lambda_1$, in the saddle homoclinic case, and as $-\ln \|\alpha - \alpha^*\|$ in the saddle-node case.

4.1.3 Three-parameter continuation

Finally, we can follow the curve of non-central saddle-node homoclinic orbits in three parameters. The extra continuation parameter is d_0 . To achieve this we restart at the codim 2 point D_1 . We return to continuation of saddle-node homoclinics, but append the defining equation $\psi_{15} = 0$ to the continuation problem. Now we have $n_s = 1$, $n_u = 0$, and three free parameters (d_0, Z, K) . Notice that we consider d_0 as the first continuation parameter, because AUTO86 detects limit points with respect to this one.

We will also detect intersections of the computed curve with the plane $d_0 = 0.01$. Running HOMCONT reveals a limit point with

$$d_0 = 0.01081235 \dots,$$

at which value the homoclinic curve P touches the branch t_2 of fold bifurcations. Beyond this value of d_0 , P consists entirely of saddle homoclinic orbits. The data at the intersection point with the plane $d_0 = 0.01$ reproduces the coordinates of the point D_2 . The results of

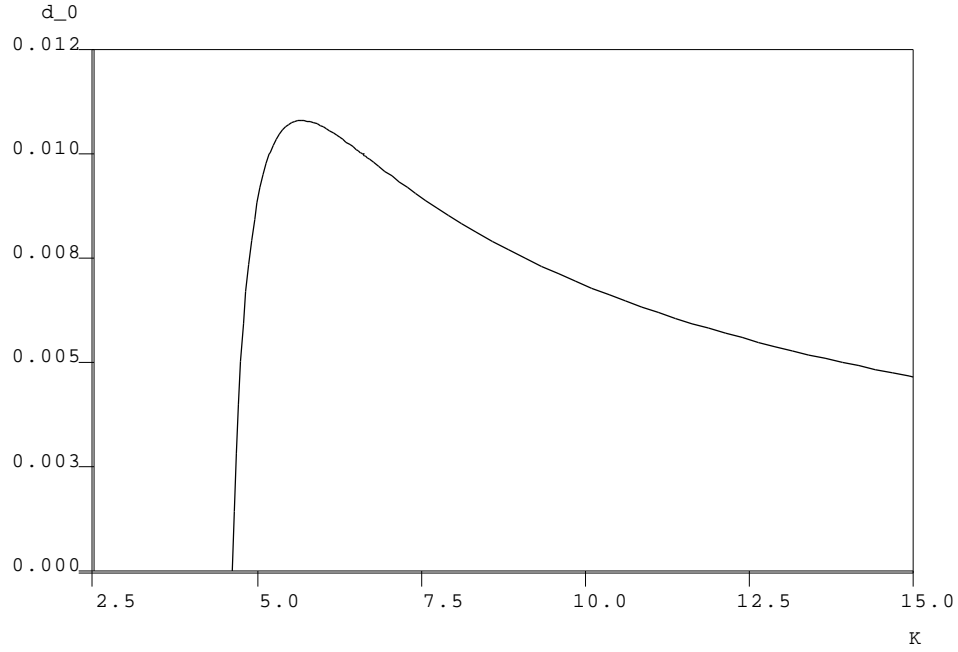


Figure 6: Projection onto the (K, d_0) -plane of the three-parameter curve of non-central saddle-node homoclinic orbits

this computation and a similar one starting from D_1 in the opposite direction are displayed in Figure 6.

4.2 Koper's extended Van der Pol model

This section deals with the equations (Koper 1994)

$$\dot{x} = \varepsilon_1^{-1} (k y - x^3 + 3x - \lambda), \quad (4.3)$$

$$\dot{y} = x - 2y + z, \quad (4.4)$$

$$\dot{z} = \varepsilon_2(y - z). \quad (4.5)$$

To begin with we fix $\varepsilon_1 = 0.1$ and $\varepsilon_2 = 1$.

4.2.1 The primary branch of homoclinics

First, we solve for a homoclinic orbit using the homotopy method. We begin with continuation in T starting from $T = 0.1$ and using approximate parameter values for a homoclinic orbit in (4.3)–(4.5), namely

$$\lambda = -1.851185, \quad k = -0.15,$$

at which the corresponding saddle is located at

$$x = y = z = -0.9591016 \dots$$

The output shows that the right-hand projection boundary condition is satisfied at

$$T = 19.08778 \dots$$

However, upon plotting the corresponding data (see Figure 7(a)) it can be noted that although the right-hand projection boundary condition is satisfied, the right-hand endpoint of the solution is still quite a way from the equilibrium. The endpoint can be made to approach the equilibrium by performing a further continuation in T with the right-hand projection condition applied but with λ allowed to vary. Running HOMCONT again one can see that

$$T = 60.0$$

provides a good approximation to a homoclinic solution (see Figure 7(b)).

The second stage for obtaining a starting solution for a homoclinic bifurcation analysis is to add a solution of the modified adjoint variational equation. This is done by a simple two-step process. First we use a support routine from HOMCONT to add some trivial data to that defining the homoclinic orbit with $T = 60.0$. Then we perform a single continuation step in a dummy parameter in order to solve the modified adjoint equation (see Section 3.3). The output contains the homoclinic solution and the solution of the adjoint equation. We now have a starting solution and are ready to perform a two-parameter continuation in (λ, k) while monitoring the test functions $\psi_{13,14}$ for an inclination flip and the test functions $\psi_{9,10}$ for a nonhyperbolic equilibrium.

Among the output we find two zeros of the test function ψ_{13} , which gives the accurate location of two inclination-flip bifurcations:

$$(\lambda^1, k^1) = (-1.801663 \dots, -0.2002655 \dots)$$

and

$$(\lambda^2, k^2) = (-1.568756 \dots, -0.4395466),$$

and a point at which the equilibrium undergoes a saddle-node bifurcation (a zero of the test function ψ_9), namely a non-central saddle-node homoclinic orbit at

$$(\lambda^3, k^3) = (0.1765060 \dots, -2.405332 \dots).$$

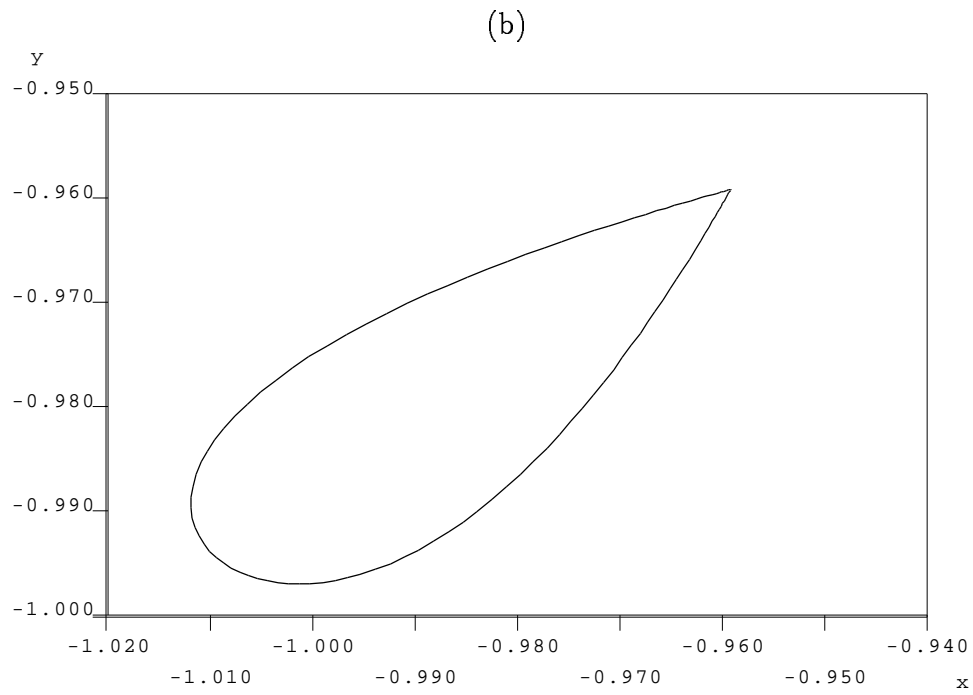
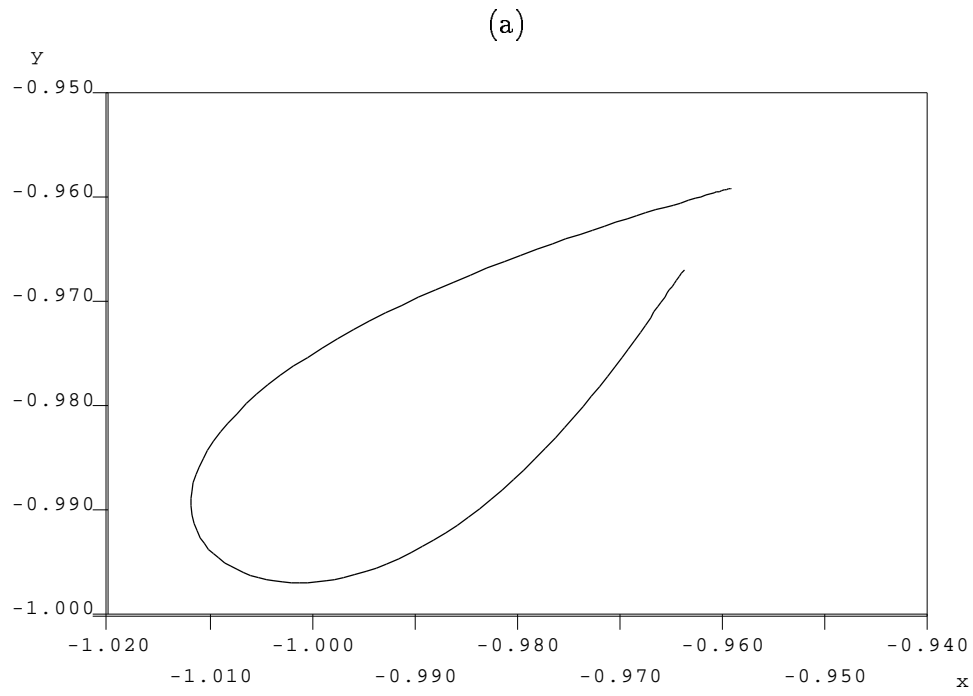


Figure 7: Projection on the (x, y) -plane of solutions of the boundary-value problem with (a) $2T = 19.08778$; (b) $2T = 60.0$

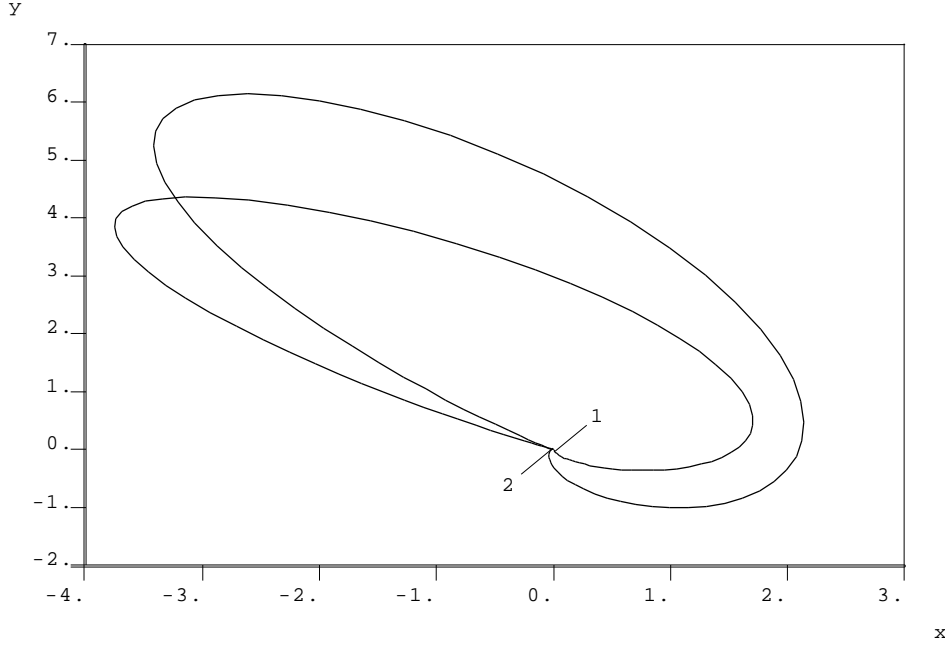


Figure 8: Projection on the (x, y) -plane of solutions $\varphi(t)$ at $(\lambda, k) = (-1.825470, -0.1760749)$ (label 1) and at $(\lambda, k) = (-1.686154, -0.3183548)$ (label 2)

Note that in Koper (1994) only the first inclination-flip point was found. However, the second flip explains the bifurcation picture drawn in (Koper 1994, Figure 11) much better when compared with the theoretical predictions. Actually, it seems as if each of the N -homoclinics bifurcating from the first flip point undergoes an inclination-flip itself for a parameter value close to the second flip point. A detailed investigation is left for future work.

Figure 8 presents solutions $\varphi(t)$ of the modified adjoint variational equation (see Section 2.2.2) at labels 1 and 2 which are points on the homoclinic branch before and after the first detected inclination flip. Note from the blow-up in Figure 9 that the directions of approach of these solutions to the origin in forwards time are approximately opposite, whereas the directions of departure are approximately the same⁵. This accords with the theoretical properties of $\varphi(t)$ at an inclination flip bifurcation (see Section 2.2.2 and references therein), which may be regarded as being like an “orbit-flip bifurcation” for $\varphi(t)$ rather than for the homoclinic orbit itself. Note that the data in Figure 8 were plotted after first performing an additional continuation of the solutions at both points with respect to the truncation interval T .

Continuing in the other direction, we approach a Bogdanov-Takens point. Phase portraits

⁵The reason why these directions are not exactly opposite or the same, respectively, is that the eigenvectors of A^T move as the parameters vary along the homoclinic curve.

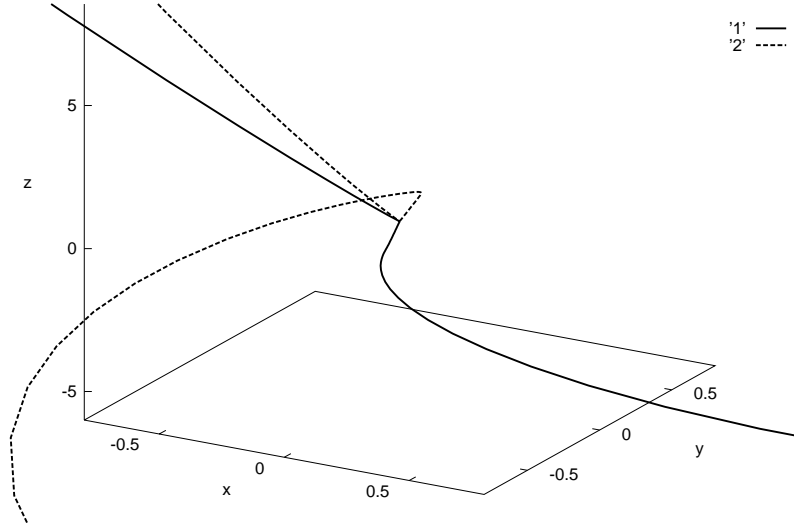


Figure 9: Three-dimensional blow-up of the solution curves $\varphi(t)$ at label 1 (solid line) and label 2 (dotted line)

of homoclinic orbits between the first inclination flip and the BT point are depicted in Figure 10, note how the computed homoclinic orbits approaching the BT point have their endpoints well away from the equilibrium. This shows that we need to take a larger truncation interval.

4.2.2 More accuracy and saddle-node homoclinic orbits

To analyse the branch of homoclinic orbits further, we first perform continuation in T from one point on the previously computed branch in order to obtain an approximation of the homoclinic orbit over a longer interval. This is necessary for parameter values near a non-hyperbolic equilibrium (either a saddle-node or BT point) where the convergence to the equilibrium is slower. First, we pick a point well away from the non-hyperbolic equilibria, remove the data for the computation of the modified adjoint variational equation, and continue in T until

$$T = 985.5682.$$

We can now repeat the computation of the branch of saddle homoclinic orbits from this point. The saddle-node point is now detected at

$$(\bar{\lambda}^3, \bar{k}^3) = (0.1764948 \dots, -2.405358 \dots).$$

Note that the parameter values differ from those at the previously-computed saddle-node homoclinic point only in the fifth decimal place. Rerunning in the opposite direction results in a

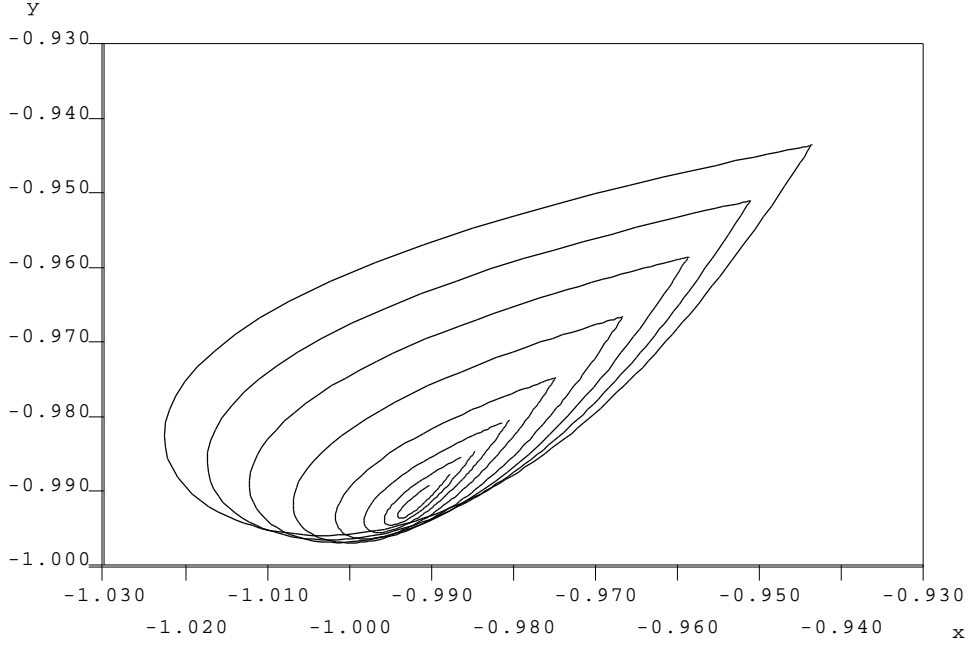


Figure 10: Computed homoclinic orbits approaching the BT point

more accurate approximation to the curve of homoclinics approaching the *BT* point:

$$(\lambda^0, k^0) = (-1.950577, -0.04962832).$$

Now we can switch to continuation of the central saddle-node homoclinic curve in two parameters, from the non-central saddle-node homoclinic orbit at $(\bar{\lambda}^3, \bar{k}^3)$. Upon running, we see that at

$$(\lambda^4, k^4) = (0.1764896, -2.405369 \dots).$$

the branch of homoclinic orbits once again leaves the locus of saddle-nodes in a second non-central saddle-node homoclinic bifurcation (a zero of ψ_{16}). Plotting a phase space diagram (see Figure 11) shows clearly that, between the two codimension-two points (labels 1 and 3), the homoclinic orbit rotates between the two components of the one-dimensional stable manifold, i.e. between the two boundaries of the center-stable manifold of the saddle node. The overall effect of this process is the transformation of a nearby “small” saddle homoclinic orbit to a “big” saddle homoclinic orbit (i.e. with two extra turning points in phase space).

Finally, we can switch to continuation of the big saddle homoclinic orbit from the new codim 2 point (λ^4, k^4) . The computed approaches the point $(\lambda, k) = (0, -2.190 \dots)$. By plotting phase portraits of computed orbits near this point (see Figure 12) we see a “canard-like” transformation of the big homoclinic orbit to a pair of homoclinic orbits in a figure-of-eight

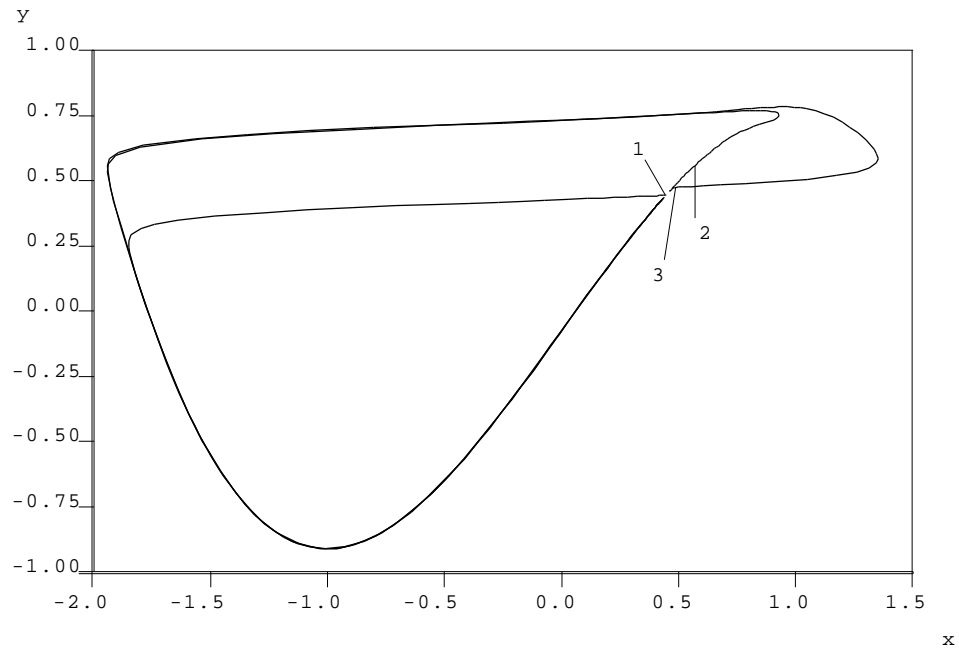


Figure 11: Two non-central saddle-node homoclinic orbits at $(\bar{\lambda}^3, \bar{k}^3)$ and (λ^4, k^4) (labels 1 and 3, respectively), and a central saddle-node homoclinic orbit between these two points (label 2).

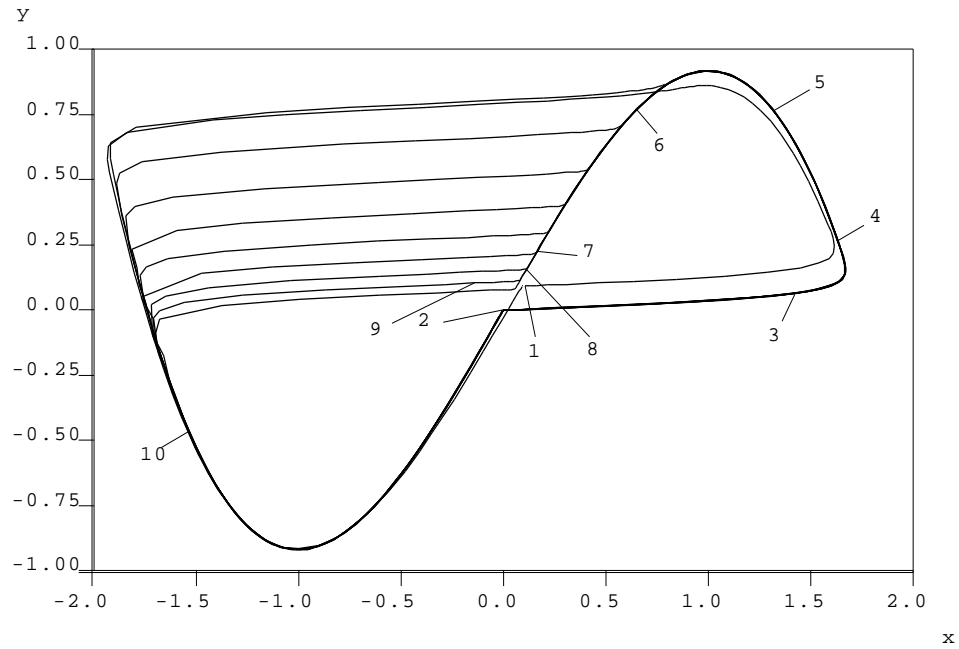


Figure 12: The big homoclinic orbit approaching a figure-of-eight (labels 1 to 10)

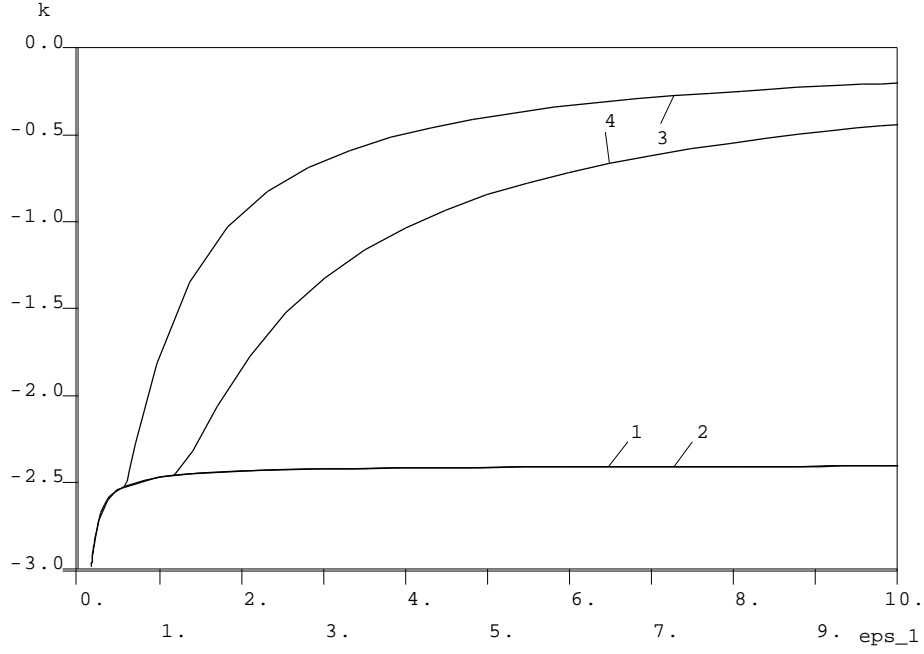


Figure 13: Projection onto the (ε_1, k) -plane of the non-central saddle-node homoclinic orbit curves (labelled 1 and 2) and the inclination flip curves (labelled 3 and 4).

configuration. That we get a figure-of-eight is not a surprise because $\lambda = 0$ corresponds to a symmetry in the differential equations (Koper 1994); note also that the equilibrium approaches the origin as we approach the figure-of-eight homoclinic.

4.2.3 Three parameter continuation

We now consider curves in three parameters of each of the codimension-two points encountered in Section 4.2.2, by freeing the parameter ε_1 in (4.3)–(4.5). The continuation in three parameters of the first inclination flip detected gives a codimension-three point (a zero of ψ_9) where the neutrally twisted homoclinic orbit collides with the saddle-node curve

$$(\lambda, k, \varepsilon_1) = (0.1282702 \dots, -2.519325 \dots, 0.5744773 \dots).$$

Continuing the other detected inclination flip, we find a point at which this branch of inclination flips collides with that of the non-central saddle-node homoclinic orbits

$$(\lambda, k, \varepsilon_1) = (0.1535420, -2.458100 \dots, 1.171705 \dots).$$

To continue the non-central saddle-node homoclinic orbits it is necessary to work on the data without the solution $\varphi(t)$. We could continue these codim 2 points in two ways, either by

appending the defining condition $\psi_{16} = 0$ to the continuation of saddle-node homoclinic orbits, or by appending $\psi_9 = 0$ to the continuation of a saddle homoclinic orbit. The first approach was used in the example in Section 4.1.3, for contrast we shall adopt the second approach here. The projection onto the (ε_1, k) -plane of all four of these codimension-two curves is given in Figure 13. The intersection of the inclination-flip lines with one of the non-central saddle-node homoclinic line is apparent. Note that the two non-central saddle-node homoclinic orbit curves are almost overlaid.

5 Conclusion

This paper has presented a toolbox for homoclinic bifurcation analysis, collecting and extending various recent developments. The resulting software, called HOMCONT, allows one to continue saddle and saddle-node homoclinic orbits satisfying certain conditions, in two or more parameters, and to switch easily between different continuation problems.

In fact, although not mentioned above, HOMCONT also supports the continuation of heteroclinic orbits connecting two hyperbolic equilibria in an appropriate number of free parameters depending on the codimension of the connection. However, none of the test functions provided are specifically designed for such orbits.

We have also ignored explicit reference to systems with special properties like equivariance, reversibility or Hamiltonian structure. In some cases, such a system provides no extra complications, for example when an orbit is not invariant under a discrete symmetry or reversibility transformation under which the underlying differential equation is invariant. In this case we simply continue one of the symmetry-coupled homoclinic orbits. However, certain test functions may not have meaning in these situations. The case when the homoclinic orbit is invariant requires separate treatment (see Champneys & Spence (1993) for reversible homoclinic orbits and Aronson, van Gils & Krupa (1994) for some results on inclination flips in systems with \mathbb{Z}_2 -symmetry).

In the case of Hamiltonian systems, homoclinic orbits appear in continua, thus the basic problem is that of one-parameter continuation. Given a system of the form

$$\dot{x} = J\nabla H(x, \alpha), \quad x \in \mathbb{R}^{2n}, \quad \alpha \in \mathbb{R},$$

where J is the usual skew-symmetric $(2n \times 2n)$ matrix, one can however use a trick employed by Beyn (1990b) which consists of performing two-parameter continuation in (α, ε) of a non-

degenerate homoclinic orbit of the modified system

$$\dot{x} = J\nabla H(x, \alpha) + \varepsilon \nabla H(x, \alpha).$$

Here ε is an artificial parameter which is zero along the true homoclinic branch. One could then use HOMCONT directly on the modified system.

As already mentioned there are many codim 2 or higher degeneracies of homoclinic bifurcations that we have not treated, notably cases involving multiple homoclinic orbits or collision between the homoclinic orbit and another invariant set (e.g. another equilibrium or a limit cycle). We have also not discussed the possibility of branch switching to bifurcation curves emanating from codim 2 homoclinic bifurcations. In particular, there are several cases where curves of *double* homoclinic orbits bifurcate from the primary one (see Champneys & Kuznetsov (1994) and references therein). In some cases the emanating curves are *exponentially close* to the primary homoclinic branch, locally. One approach to treating both this problem and the computation of homoclinic orbits approaching heteroclinic cycles is to be able to solve coupled pairs of boundary value problems, defining two separate pieces of a single orbit and to be able to switch between double and single boundary value problems.

We hope that the presented toolbox will prove useful for both applications and for the development of new theoretical results and numerical algorithms for global bifurcations.

6 Acknowledgements

The authors acknowledge the support of a Nuffield Foundation “Newly Appointed Science Lecturer” grant and a visiting fellowship grant from the EPSRC, UK.

References

- Aronson, D., van Gils, S. & Krupa, M. (1994), ‘Homoclinic twist bifurcations with \mathbb{Z}^2 symmetry’, *J. Nonlinear Sci.* **4**, 195–219.
- Bai, F. & Champneys, A. (1994), Numerical detection and continuation of saddle-node homoclinic bifurcations of codimension one and two, Technical report, University of Bath. Mathematics Preprint 94-04.
- Belyakov, L. & Shil’nikov, L. (1990), ‘Homoclinic curves and complex solitary waves’, *Selecta Mathematica Sovietica* **9**, 219–228.

- Beyn, W.-J. (1990*a*), Global bifurcations and their numerical computation, *in* D. Roose, A. Spence & B. De Dier, eds, ‘Continuation and Bifurcations: Numerical Techniques and Applications’, Kluwer, Dordrecht, Netherlands, pp. 169–181.
- Beyn, W.-J. (1990*b*), ‘The numerical computation of connecting orbits in dynamical systems’, *IMA J. Num. Anal.* **9**, 379–405.
- Canale, V. (1994), The computation of paths of homoclinic orbits, PhD thesis, Department of Computer Science, University of Toronto.
- Champneys, A. & Kuznetsov, Y. (1994), ‘Numerical detection and continuation of codimension-two homoclinic bifurcations’, *Int. J. Bifurcation & Chaos* **4**, 795–822.
- Champneys, A. & Spence, A. (1993), ‘Hunting for homoclinic orbits in reversible systems: a shooting technique’, *Adv. Comp. Math.* **1**, 81–108.
- Champneys, A., Härterich, J. & Sandstede, B. (1995), ‘A non-transverse homoclinic orbit to a saddle-node equilibrium’, *Ergodic Theory and Dynamical Systems*. To appear.
- Champneys, A., Kuznetsov, Y. & Sandstede, B. (1995), HOMCONT: An AUTO86 driver for homoclinic bifurcation analysis. Version 2.0, Technical report, CWI, Amsterdam. To appear.
- Chow, S.-N., Deng, B. & Fiedler, B. (1990), ‘Homoclinic bifurcation at resonant eigenvalues’, *J. Dyn. Diff. Eqs.* **2**, 177–244.
- Deng, B. (1993), ‘Homoclinic twisting bifurcations and cusp horseshoe maps’, *J. Dyn. Diff. Eqs.* **5**, 417–468.
- Doedel, E. (1981), ‘AUTO, a program for the automatic bifurcation analysis of autonomous systems’, *Cong. Numer.* **30**, 265–384.
- Doedel, E. & Friedman, M. (1989), ‘Numerical computation of heteroclinic orbits’, *J. Comp. Appl. Math.* **26**, 159–170.
- Doedel, E. & Kernévez, J. (1986), AUTO: Software for continuation problems in ordinary differential equations with applications, Technical report, California Institute of Technology. Applied Mathematics.

- Doedel, E., Friedman, M. & Monteiro, A. (1993), On locating homoclinic and heteroclinic orbits, Technical report, Cornell Theory Center; Center for Applied Mathematics, Cornell University.
- Doedel, E., Keller, H. & Kernévez, J. (1991*a*), ‘Numerical analysis and control of bifurcation problems: (I) Bifurcation in finite dimensions’, *Int. J. Bifurcation and Chaos* **1**, 493–520.
- Doedel, E., Keller, H. & Kernévez, J. (1991*b*), ‘Numerical analysis and control of bifurcation problems: (II) Bifurcation in infinite dimensions’, *Int. J. Bifurcation and Chaos* **1**, 745–772.
- Fiedler, B. (1992), Global pathfollowing of homoclinic orbits in two-parameter flows, Technical report, Institut für Angewandte Analysis und Stochastik, Berlin. Applied Mathematics.
- Friedman, M. (1993), ‘Numerical analysis and accurate computation of heteroclinic orbits in the case of center manifolds.’, *J. Dyn. Diff. Eqs* **5**, 59–87.
- Friedman, M. & Doedel, E. (1991), ‘Numerical computation and continuation of invariant manifolds connecting fixed points’, *SIAM J. Numer. Anal.* **28**, 789–808.
- Friedman, M. & Doedel, E. (1993), ‘Computational methods for global analysis of homoclinic and heteroclinic orbits: A case study’, *J. Dyn. Diff. Eqs.* **5**, 37–57.
- Gaspard, P., Arnéodo, A., Kapral, R. & Sparrow, C., eds (1993), *Homoclinic Chaos, Physica D* **62** (1-4), special issue.
- Golub, G. & van Loan, C. (1989), *Matrix Computations (second edition)*, John Hopkins University Press, Baltimore.
- Hassard, B. (1980), Computation of invariant manifolds, *in* P. Holmes, ed., ‘New Approaches to Nonlinear Problems in Dynamics’, SIAM, pp. 27–42.
- Homburg, A., Kokubu, H. & Krupa, M. (1994), ‘The cusp horseshoe and its bifurcations from inclination-flip homoclinic orbits’, *Ergodic Theory and Dynamical Systems* **14**, 667–693.
- Khibnik, A., Kuznetsov, Y., Levitin, V. & Nikolaev, E. (1993), ‘Continuation techniques and interactive software for bifurcation analysis of ODEs and iterated maps’, *Physica D* **62**, 360–371.

- Kisaka, M., Kokubu, H. & Oka, H. (1993), 'Bifurcation to n -homoclinic orbits and n -periodic orbits in vector fields', *J. Dyn. Diff. Eqs.* **5**, 305–358.
- Koper, M. (1994), Far-from-equilibrium phenomena in electrochemical systems, PhD thesis, Univeriteit Utrecht, Holland.
- Kuznetsov, Y. (1983), One-dimensional invariant manifolds in ordinary differential equations depending upon parameters. FORTRAN Software Series, 8, Research Computing Centre, USSR Academy of Sciences, Pushchino. In Russian.
- Kuznetsov, Y. (1990), Computation of invariant manifold bifurcations, *in* D. Roose, A. Spence & B. De Dier, eds, 'Continuation and Bifurcations: Numerical Techniques and Applications', Kluwer, Dordrecht, Netherlands, pp. 183–195.
- Lukyanov, V. (1982), 'Bifurcations of dynamical systems with a saddle-point separatrix loop', *Differential. Eq.* **18**, 1049–1059.
- Miura, R. (1982), 'Accurate computation of the stable solitary wave for the FitzHugh–Nagumo equations', *J. Math. Biol.* **13**, 247–269.
- Nozdrachova, V. (1982), 'Bifurcation of a noncourse separatrix loop', *Differential Eq.* **18**, 1098–1104.
- Rodríguez-Luis, A., Freire, E. & Ponce, E. (1990), A method for homoclinic and heteroclinic continuation in two and three dimensions, *in* D. Roose, A. Spence & B. De Dier, eds, 'Continuation and Bifurcations: Numerical Techniques and Applications', Kluwer, Dordrecht, Netherlands, pp. 197–210.
- Sandstede, B. (1993), Verzweigungstheorie homokliner Verdopplungen, PhD thesis, Universität Stuttgart.
- Sandstede, B. (1995*a*), Constructing dynamical systems possessing homoclinic bifurcation points of codimension two, In Preparation.
- Sandstede, B. (1995*b*), Convergence estimates for the numerical approximation of homoclinic solutions, In Preparation.
- Sandstede, B. (1995*c*), Numerical computation of homoclinic flip-bifurcations, In Preparation.

- Schechter, S. (1993), ‘Numerical computation of saddle-node homoclinic bifurcation points’, *SIAM J. Num. Anal.* **30**, 1155–1178.
- Schechter, S. (1994), Rate of convergence of numerical approximations to homoclinic bifurcation points, North Carolina State University.
- Scheffer, M. (1995), ‘Personal communication’.
- Shil’nikov, L. (1969), ‘On a new type of bifurcation of multidimensional dynamical systems’, *Sov. Math. Dokl.* **10**, 1368–1371.
- Turaev, D. (1988), ‘On the bifurcations of a homoclinic ‘figure eight’ of a multidimensional saddle’, *Russ. Math. Surv.* **43**, 264–265.